encit 2020

ABCM Associação Brasileira de Engenharia e Ciências Mecânicas

18th Brazilian Congress of Thermal Sciences and Engineering
November 16-20, 2020 (online)

ENC-2020-0256
OPTIMIZATION DESIGN METHOD FOR WIND TURBINE AIRFOILS CONSIDERING DIFFERENT ANGLES OF ATTACK OVER NACA 0012.

Eduardo Pavoni Gamba[1]
Rodrigo C. Palharini[2]
Instituto de Aeronáutica e Espaço, 12228-904, São José dos Campos, SP, Brazil
Department of Mechanical Engineering, Universidad Técnica Federico Santa María, Santiago, Chile
eduardopg@ita.br, rodrigo.cassineli@usm.cl

Abstract. *Energy generation has led the world to deal with serious environmental damages. However, energy from wind is a clean renewable source which is promising for diminishing these problems. Some previous effort has been made to increase wind power production by designing more efficient airfoils. In doing so, the main objective of this work is to employ the adjoint optimization method and CFD simulations to improve the design and efficiency of wind turbine blade airfoils. The main parameter investigated in this work is the influence of the optimization's angle of attack on the resulted airfoil. The first step to achieve the main goal was to perform the validation process of the CFD by comparing numerical simulations to wind tunnel results. Next, the adjoint optimization method was tested for different meshes in order to verify the model's results coherence. Finally, the optimization and simulations were performed for NACA 0012 airfoil at different angles of attack. The results from the optimized airfoils were compared to the not optimized through their efficiency curves. According to the results, it was observed an increase of 8.5 % in the efficiency when the optimized airfoil is considered.*

Keywords: *wind power airfoils, optimization, numerical validation, CFD, angle of attack.*

1. INTRODUCTION

The growing concerns about environmental impacts and energy crises around the world have led to massive investments in the development of renewable energy sources. Among these energy sources, wind power generation has been growing sharply. Brazil has an energy matrix based on hydraulic power extraction, which has its environmental issues related. In this scenario, wind power emerges as alternative for energy matrix diversification. However, it brings to light the importance of improving wind turbines efficiency due the wind regimes in Brazil. A high-performance airfoil for wind turbine blades is a parameter that still requires more attention. Only a few investigations have focused in blade optimization and some of those are described as follow:

Ribeiro et al. (2012) stated that airplanes airfoils are used for wind power applications, even though the criteria are not the same, and the Reynolds and Mach number are much lower for wind turbines. Thus, they applied a genetic algorithm and computational fluid dynamics (CFD) to optimize wind turbine airfoils. They concluded that 2D steady incompressible RANS with the Spalart-Allmaras turbulence model was effective for wind turbine airfoil design. Nevertheless, the usage of genetic algorithms often requires a high number of iterations and it is time-consuming when high-fidelity CFD and this optimization method are applied together.

Polat and Tuncer (2013) developed an aerodynamic shape optimization methodology using a genetic algorithm and Blade Element Momentum theory for horizontal axis wind turbines. For the aerodynamic analyses, they used the potential flow solver with a boundary layer model, XFOIL. The blade sections were defined by the NACA four-digit airfoil series or by arbitrary profiles defined by a Bezier curve. An optimization study was conducted on the baseline NordTank turbine with 43 design variables, a wind speed of 10 m/s and population size 10. The NACA airfoils were selected for root, mid-span and tip regions. The design process achieved about a 10% increase in power production, calculated by the BEM theory.

Chen et al. (2015) also defended that the development of wind turbine airfoils was built upon the aircraft airfoils to some extent, such as NACA and FX series. According to them, one key element in the aerodynamic design of wind turbine blades is the use of specially tailored airfoils to improve the ratio of energy capture and to reduce the cost of energy. It is well known that the aerodynamic design of wind turbine blades is mainly concerned with the airfoil design.

They performed a wind turbine airfoil design combining a genetic algorithm and the flow solver RFOIL. The objective of the airfoil optimization was to maximize the lift/drag ratio at a design angle of attack with airfoil thickness ranging from 15 to 20% for structural reasons. A high-order Tylor series was proposed to represent the shape function. Three airfoils with high aerodynamic performance were designed by controlling the coefficients of the shape function,

named WT airfoils families. The new airfoils showed better aerodynamic performances when compared to some commonly used wind turbine airfoils.

Alternatively, Schramm et al. (2014) used a gradient-based optimization for the problem of wind turbine design. This approach leads to fewer iterations when compared to genetic algorithms. The study chose the adjoint optimization method due to its capability to work with large numbers of design variables with additional cost. The gradient-based approach is preferred for this case since they were starting from the SU 91-W2-250 profile, which is assumed to be close to the optimum.

The optimization cost function was maximized the lift to drag ratio for different angles of attack with a constant cross-section area as an additional constraint. The method was implemented in the open-source CFD code OpenFOAM with Navier-Stokes equations. For instance, good results are obtained using an initial step size of 0.001 of the chord length. The simulations use wall functions with a dimensionless wall distance of 100, and turbulence was modeled applying the k-w-SST model. The Reynolds number was 3 million and the computational grid consisted of approx. 55,000 cells, where 360 were on the airfoil. The method succeeded in improving aerodynamic efficiency. From the optimization results it was shown that a bigger distance to the initial maximum of lift to drag ratio lead to bigger changes in the aerodynamic properties. The geometric constrained could be fulfilled but with the drawback of a less improved cost function.

The main goal of this investigation is the design and optimization of wind turbine airfoils at different angles of attack (α). In in order to archive this goal, the SU2 computational code is employed since it has the adjoint optimization method and Reynolds Average Navier-Stokes (RANS) implemented into it. The aerodynamic efficiency, *E*, is set as the optimization's cost function, due to its importance to improve wind power extractions. A minimum airfoil thickness of 12% was chosen as geometry constraint for structural reasons. The Hicks-Henne bump function is used for geometry parametrizations.

2. COMPUTATION METHOD AND CFD CODE

The SU2 is a reliable open-source code developed by Stanford University and is capable of solving CFD simulations throughout the adjoint optimization design method. Thus SU2 is chosen as the computational tool for the development of this investigation. The code is divided in seven modules written in C++ and wrapped by Python script (Palacios et al., 2013). The main module's features are described below:

1) SU2_CFD: The main PDE solution module that started primarily as a Euler and RANS CFD solver, but has been modified to treat many other governing equations, including the adjoint equations for many of the supported governing equation systems.
2) SU2 DDC: The Domain Decomposition Code, used to prepare SU2 for computations involving multiple processors.
3) SU2 GPC: The Gradient Projection Code that allows for the calculation of sensitivities for use in optimization and uncertainty quantification.
4) SU2 MDC: The Mesh Deformation Code that can be used to perturb an existing unstructured volume mesh to conform to new surface geometries dictated by either shape optimization processes or aero-structural simulations.

The Navies-Stokes equations are a set of formulas based on the conservation of mass, momentum, and energy regarding a viscous fluid. The time-averaging of the flow properties leads to the Reynolds Average Navier Stokes, called RANS formulation. In benchmark CFD problems, RANS are often assumed as governing equations for the air around an airfoil, for example in Schramm et al. (2014) and Ribeiro et al. (2012). The SU2's PDE system for compressible RANS equations within a computation domain Ω is conveyed in Eq.(1) (Palacio et al., 2013). $Q(U)$ is a generic source term, $U = (\rho, \rho v_1, \rho v_2, \rho e)^T$ is the vector of conservative variables, where ρ is the air density, e is the total energy per unit mass, and v is the velocity.

$$\partial_t U + \nabla \cdot \vec{F}^c - \nabla \cdot \vec{F}^v = Q \quad in\ \Omega, t > 0 \tag{1}$$

The convective flux $\vec{F}^c(U)$ and the viscous flux $\vec{F}^v(U)$ are represented by Eq.(2).

$$\vec{F}_i^c = \begin{pmatrix} \rho v_i \\ \rho v_i v_1 + P\delta_{i1} \\ \rho v_i v_2 + P\delta_{i2} \\ \rho v_i H \end{pmatrix}, \quad \vec{F}_i^v = \begin{pmatrix} . \\ \tau_{i1} \\ \tau_{i2} \\ v_i \tau_{ij} + \mu_{tot} C_p \partial_i T \end{pmatrix}, \quad i = 1,2 \tag{2}$$

P is the static pressure, H is the fluid enthalpy, δ_{ij} is the *Kronecker* delta function, C_p is the specific heat at constant pressure, T is the temperature, and R is the gas constant. The viscous stresses are written as $\tau_{ij} = \mu_{tot}\left(\partial_j v_i + \partial_i v_j - \frac{2}{3}\delta_{ij}\nabla \cdot \vec{v}\right)$. The *Boussinesq* hypothesis (WILCOX, 1998) evaluates the effect of turbulence by dividing the total viscosity μ_{tot} into the laminar viscosity and a turbulent viscosity that must be modeled. To do that, this

work uses the Spalart-Allmaras turbulence model due to its successful use in aerodynamic optimization of airfoils (Ribeiro et al., 2012). This one equation turbulence model proposed by Spalart and Allmaras (1992) was designed specifically for aerospace applications involving wall-bounded flows.

Regarding the boundary conditions, the far-field region was considered a flow independent from the effect of the airfoil, where the freestream values for the air properties are used for the characteristic-based, non-reflecting boundary conditions. Regarding the airfoil boundary wall, no mass or any convective flux can penetrate the solid body, so the velocity in the normal direction at the airfoil is equal to zero. The relative velocity between the flow and the solid wall is also equal to zero, which is known as the no-slip condition.

This work applies the second-order, central scheme Jameson-Schmidt-Turkel to perform the integrations of the convective fluxes, while the first-order scalar upwind method is applied for the space discretization of the convective terms of the turbulence equations. With respect to the viscous fluxes, the least-squares method is used at the mesh nodes to average and calculate the gradients of the flow variables at the cell faces. Concerning the time discretization, an implicit scheme is a convenient approach to obtain stability for the CFD iteration process. In this approach, the residual is evaluated at time t^{n+1}. Therefore, this work uses the Euler Implicit scheme to discretize the governing equations with respect to time. Moreover, the present work adopts the FGMRES, which stands for Flexible Generalized Minimum Residual, to solve the linear system.

The flow condition of Reynolds equal to 3.74 e06 and Mach equal to 0.14 is assumed for the CFD simulations. These conditions represent the flow around a wind turbine blade airfoil at 90% of the span length based on the wind distribution, temperature, and other weather parameters from Salvador-BA, Brazil. The Reynolds and Mach calculations derived from the previous author's work (Gamba and Palharini, 2020) and are out of the scope of this paper.

3. OPTIMIZATION METHOD

The gradient-based method is a numeric algorithm often used for aerodynamic optimization problems. It consists of an iterative process where each step is directed towards the steeper decline direction, which is the function gradient vector. Considering an airfoil into a flow, the aerodynamics properties which define the cost function $I(w, X, F)$ are the flow field variables w, the physical locations of the mesh points within the volume X, and the physical location of the boundary F. To calculate the cost function gradient, one must solve the following equation:

$$\delta I = \frac{\delta I}{\delta w}\delta w + \frac{\delta I}{\delta X}\delta X + \frac{\delta I}{\delta F}\delta F \tag{3}$$

However, δw is not directly obtained, and it might be very expensive because the number of additional flow calculations is equal to the number of design variables. In this context, the adjoint approach is an alternative solution to reduce the excessive CPU time (Reuther, 1996). If the residual of the governing equations $R(w, X, F) = 0$ is introduced on Eq. (2), it becomes:

$$\delta I = \frac{\delta I}{\delta w}\delta w + \frac{\delta I}{\delta X}\delta X + \frac{\delta I}{\delta F}\delta F - \psi\left(\frac{\delta R}{\delta w}\delta w + \frac{\delta R}{\delta X}\delta X + \frac{\delta R}{\delta F}\delta F\right) \tag{4}$$

where the Lagrange multiplier ψ can be chosen to eliminate δw, which is known as the adjoint equation.

For the past years, it was common practice the use existing airfoil families, such as NACA series, in the design of wind turbine blades (Douvi and Margaris, 2012). Thus, the airfoil investigated in this study was the NACA 0012 airfoil. The geometry parametrization employed is the Hicks-Henne bump function due its successful applications (Reuther, 1996). In addition, the surface deformation during the optimization process is described by the following Eq. (3), where n is the number of bump functions and $x_n$the function maximum point (Palacios et al., 2013).

$$f_n(x) = sin^3(\pi x^{e_n}),\ \ e_n = \frac{log\ (0.5)}{log\ (x_n)},\ \ x \in [0,1] \tag{5}$$

The principal objective of a wind turbine optimization is to improve the power production. As demonstrated by Schramm et al. (2014), the most important airfoil feature to achieve this goal is the lift-drag ratio or aerodynamic efficiency, E. However, airfoil structural properties must be considered since the blade is exposed to intense loads. Although this work does not consider the structural analyses, a minimum airfoil thickness of 12% was set as a geometrical constraint since thick airfoils are desirable due to fatigue effects (Chen et al., 2015). Besides, step size of 0.0001 of the chord's length was adopted to maintain a realistic airfoil shape throughout the iterations.

As highlighted by Schramm et al. (2018), in some cases, the convergence of the optimization and the resulting shapes depended on the number of control points, and it is recommended that at least 30 spline control points are used. In this study, the design variables are set as surface points linearly arranged through the airfoil chord. For each 5% of chord, one design variable is defined for both upper and lower surfaces, starting from the leading edge until the trailing edge. Therefore, this work uses 40 design variables for airfoil optimization, as represented in Fig 1.

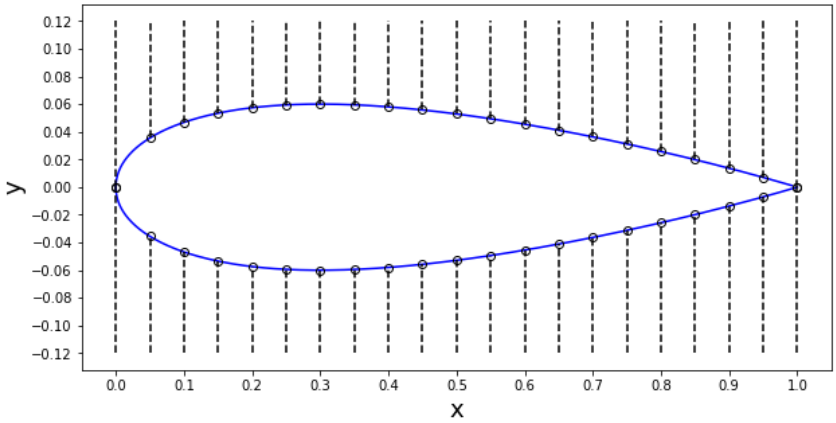

Figure 1. Design variable distribution over the airfoil surface.

4. METHODOLOGY

In this section, the methodology used in this work is discussed in detail. Firstly, it was necessary to perform the verification and validation of the computational code for the intended purpose. In this way, computational results were compared for different mesh sizes and wind tunnel data for equivalent Reynold (*Re)* and Mach (Ma). Next, the NACA 0012 airfoil was optimized following the requirements for wind turbine design and taking into account three different angles of attack.

4.1 Grid Independence Study

For the CFD simulations, it was considered a quadrangular C-shape mesh, which was built using ICEM software. In this work the dimensionless mesh parameter Y_+ was to be about 1 on the airfoil surface, then the wall distance of the first element was defined according to flat plate theory and set as 1.5e-05 m. In addition, *Spalart-Allmaras* turbulence model was applied to all simulations. In order to determine the far field distance and the grid refinement necessary to achieve reliable results, an independence grid study was carried out. Firstly, four different size of computational domains were considered, as shown in Fig. 2 a). The inlet distance was defined as 15, 30, 45 and 60 chords from the airfoil leading edge, while the outlet distances were, respectively, 25, 50, 75 and 100 chords from trailing edge.

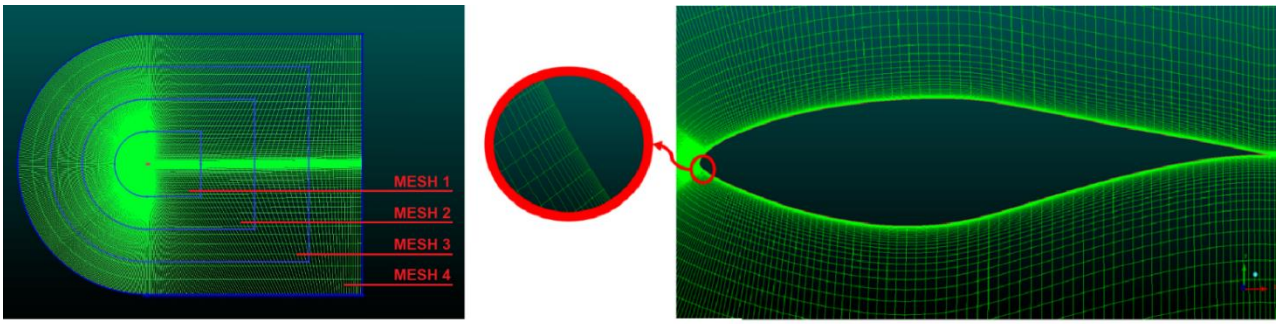

Figure 2. a) Superimposed computational meshes and b) Computational mesh around the airfoil surface.

Figure 2 b) shows the mesh near to the airfoil surface. For the grid refinement study, the number of vertexes of the standard mesh was doubled homogenously. The *Richardson* extrapolation theory (Richardson and Gaunt, 1997) was used to estimate the called exact solution for C_l and C_d values i.e., the solution considering the most refinement possible or vertex distances tending to zero. Equation (6) represents the exact solution based on the standard mesh (f_1) and refined mesh solutions (f_2). The parameter r represents the ratio of refinement and it was set equal to 2.

$$f_{exact} = f_1 + \frac{f_1 - f_2}{r^2 - 1} \tag{6}$$

The wind turbine airfoil S809, designed in the National Renewable Energy Laboratory, was chosen for the grid and far-field independence study. In the grid Independence study, the exact solution was chosen as reference and the bigger

far-field was considered as reference in the far-field Independence. In both investigation, the angle of attack was set equal to 9.22º. Table 1 shows the lift and drag coefficients for the four domains sizes considered in this study. It is noticed that Mesh 1 diverges considerably from reference values. Its percentage errors were the only to extrapolate the acceptable limit imposed of 5% given by Surki et al. (2009). From Mesh 2, it was achieved satisfactory far-field distance independence. Therefore, the mesh with 30 chords length was chosen as far-field independent.

Table 1. Drag and lift coefficients for different far-field sizes.

Mesh	C_l		C_d	
	Calculated	**% Error**	**Calculated**	**% Error**
1	1.157769	-0.283276	0.021935	8.42808
2	1.161021	-0.003187	0.020793	2.78300
3	1.160951	-0.009216	0.020455	1.11221
4	1.161058	-	0.020230	-

For the grid refinement independence study, the number of vertices was doubled, reducing the mesh element sizes by half along all the domain regions. Both meshes, standard and refined, were simulated within the same model and used for Richardson's exact solution estimation, which was set as reference. All three results are expressed on Table 2. The standard mesh, previously designed with a ratio growth of 1.15, showed the highest percentage error of 3.6%. Thus, the standard mesh satisfied the acceptable limit, reaching enough grid refinement independence. Therefore, it was not needed to refine the mesh, which would increase the computational cost.

Table 2. Mesh refinement independence study results.

	C_l		C_d	
	Calculated	**% Error**	**Calculated**	**% Error**
Standard mesh	1.161058	1.36261	0.02023	3.6196
Refined mesh	1.149352	0.34065	0.0197	0.9049
Exact solution	1.14545	-	0.019523	-

4.2 CFD validation

The validation of the computational code is a necessary step in this investigation in order to ensure that the code is reliable for the intended purpose. The main idea of the validation process is to compare the computational data with experimental measurements in order to ensure that the simulation capture the correct physics of the problem. In this way, the computed results obtained in the present work were compared with experimental data available NACA 0012 airfoil (Ladson, 1988). At these experiments, lift and drag coefficients were measured for angles of attack ranging from -4º to 18º and Reynolds and Mach number of 3.94e06 and 0.15, respectively.

Figure 3 shows the lift and drag coefficients for the NACA 0012 experimental data and computations results. The SU2 computed results are represented by red circles while the experimental data is depicted by black circles. According to the results, it is noticed an agreement between the computational and experimental data for angles of attack raging from -4º to 15º. However, for higher angles of attack, where stall is noticeable, a significant difference is observed. In this way, the computed results showed that SU2 successfully captured the NACA 0012 aerodynamic performance and computation code was considered validated for a wide range of angles of attack and freestream conditions specified in the present work.

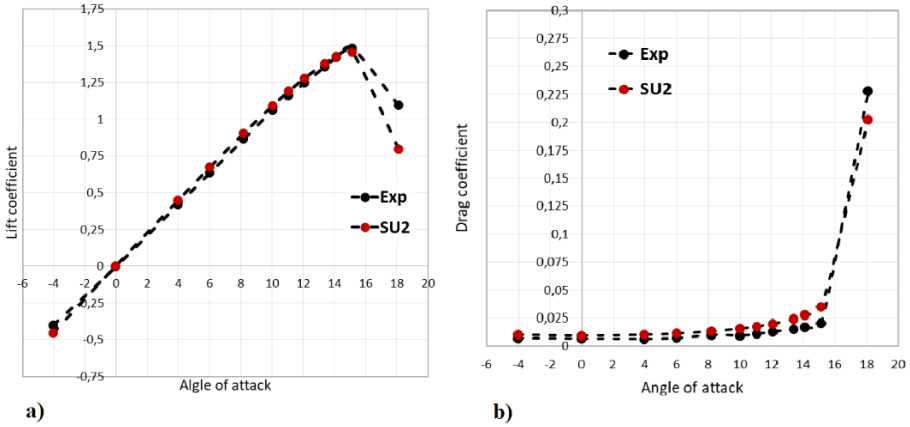

Figure 3. a) C_l vs α b) C_d vs α for wind tunnel and numerical analyses.

4.3 Validation of the adjoint optimization method

In contrast to the CFD validation performed in the previous sections, it is not possible to compare numerical results with experiments for the optimization process. Given that, the AIAA aerodynamic design optimization discussion group (ADODG) proposed several benchmarks optimization problems to provide a foundation for rational assessment of the multitudinous aerodynamic design optimization methods to problems of interest. Among the benchmark problems, the Drag Minimization of the RAE 2822 in Transonic Viscous Flow is the most similar to this work's case. The problem statement is defined as minimizing the drag coefficient of the RAE 2822 at a freestream Mach number of 0.734, a lift coefficient of 0.824, and Reynolds number of 6.5e06 subject to an area and pitching moment constraint.

The adjoint optimization method from SU2 was used to perform this benchmarks case with the same numerical model previously described. The mesh used for this validation is the RAE 2822 transonic mesh available in the SU2 official directory because the flow regime is considerably different from wind turbines' conditions. The mesh has a circular shape domain, and its elements are a hybrid mix of triangle and quadrilaterals in the airfoil's neighborhood, as illustrated in Fig. 4.

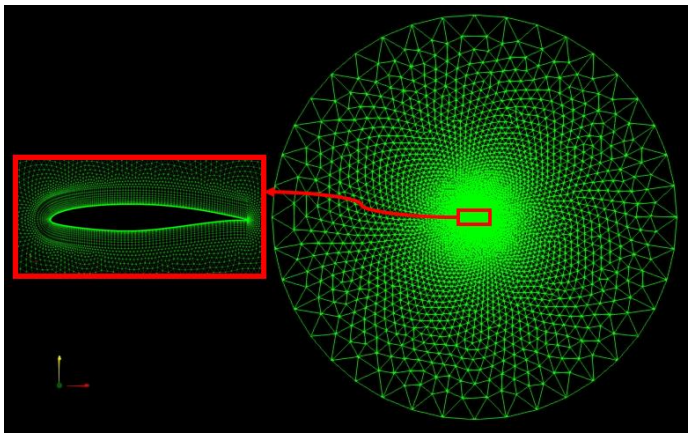

Figure 4. Test Case computational mesh.

Figure 5 represents a superposition of the pressure coefficient distribution, C_p, on the optimized airfoils. The baseline C_p distribution is reproduced by the dashed line. The presence of the shock wave on the upper surface is distinguished by the slope pressure decline between 0.5 chord and 0.6 chord. As suspected, the general behavior of the optimizations was the attempt to smooth this decline. This work's method, Wu et al., and Zhang et al. successfully quenched the shock wave appearance, as it is seen by the smooth pressure decay from the leading edge to the trailing edge. In the other two optimizations, the shock wave was dampened, yet an abrupt pressure variation remains on the airfoil's surface. Another observed general behavior is the generation of a suction peak at the leading edge. While the baseline C_p increases until the upper surface midpoint before reducing until the trailing edge, the optimized airfoils only diminish pressure from leading to the trailing edge. Given that, the author considered the optimization method of the present work validated and appropriate to be used in further analyses.

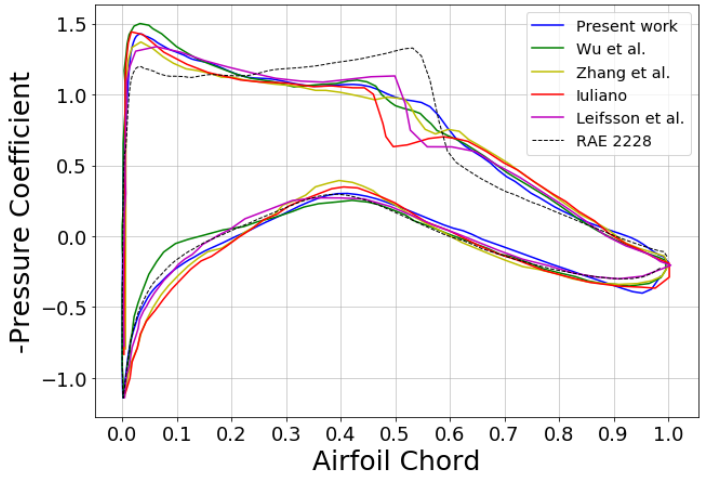

Figure 5. Comparison of benchmark pressure results by different methods.

5. COMPUTATION RESULTS

In section, the optimization process is applied to NACA 0012 airfoil at angles of attack of 5º, 7º, and 9º, be respectively referred to as OPT5, OPT7, and OPT9. During the simulation and optimization process, the trailing edge was considered as fixed point which lead to unrealistic shapes at this region. In doing so, it was necessary to correct the trailing edge position after optimization in order to adjust the camber. The optimized airfoils and NACA 0012 airfoil are shown in Fig. 6. It is observed at this plot a significant change on the airfoils thickness as the angle of attack is increased. The airfoils thickness was steeper for lower angles of attack and slight changes in the angle of attack was responsible for significant differences in the geometry shape.

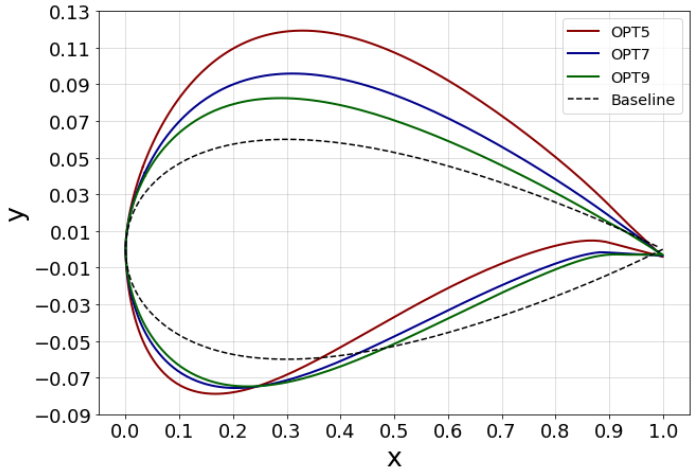

Figure 6. Optimized and original airfoil geometries.

Figure 7 a), shows the aerodynamic efficiency (E) for the three angles of attack during the simulation time. Along the iterations, it is noticed that the airfoil optimization for α = 5º demonstrated the lowest efficiency value. Concerning the other cases, their efficiency difference diminished over the iterations. After the trailing edge adjustment, the efficiency values sharply increased, which shows the usefulness of this modification. Figure 7 b) standardizes the optimizations by evaluating the percentage E growth. In this plot, it is observed higher percentage gain α = 5º. The optimization method resulted in an increase of 27% of the efficiency for this case. For the highest angle of attack investigated in this work, α = 9º, it was obtained increase of 7% in the aerodynamic efficiency.

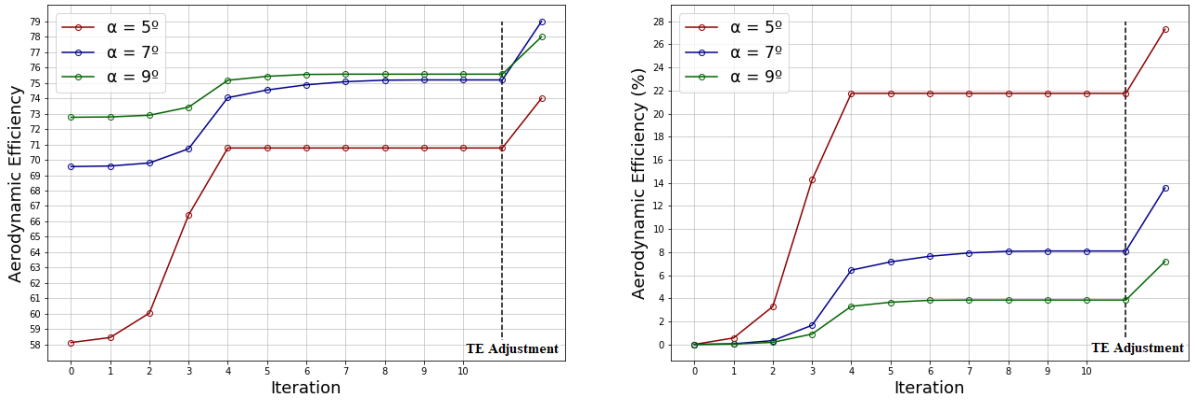

Figure 7. a) Aerodynamic efficiency gains vs. iterations and b) Percentage aerodynamic efficiency gain vs. iterations.

A comparison between the streamlines of OPT5 and OPT9 airfoils was made in Fig. 8 a) to exhibit their aerodynamic behavior and explain the optimization characteristics. It is notable that the flow reaches OPT9 at a further point in the lower surface than the OPT5 case, which forces the flow to turn around the trailing edge. It suggests that if OPT9 had experienced more expressive modifications in camber and thickness, it could have caused the beginning of stall, and that would be the reason why higher angles of attack had fewer shape modifications.

Aiming to verify if high thickness and camber would have poor performance at high angles of attack, the OPT5 airfoil was subjected to a simulation with $\alpha = 9°$. Figure 8 b) depicts the streamlines of this simulation. As it is evidenced by the red circle, there was an unattachment of the boundary layer at the trailing edge region. This recirculation indicates the beginning of the stall, and it jeopardizes the aerodynamic performance of the airfoil. The result strengthens the hypothesis that the optimized shapes for higher angles were less altered because it would induce flow unattachment, and it helps to understand the effects of the angle of attack over the optimization.

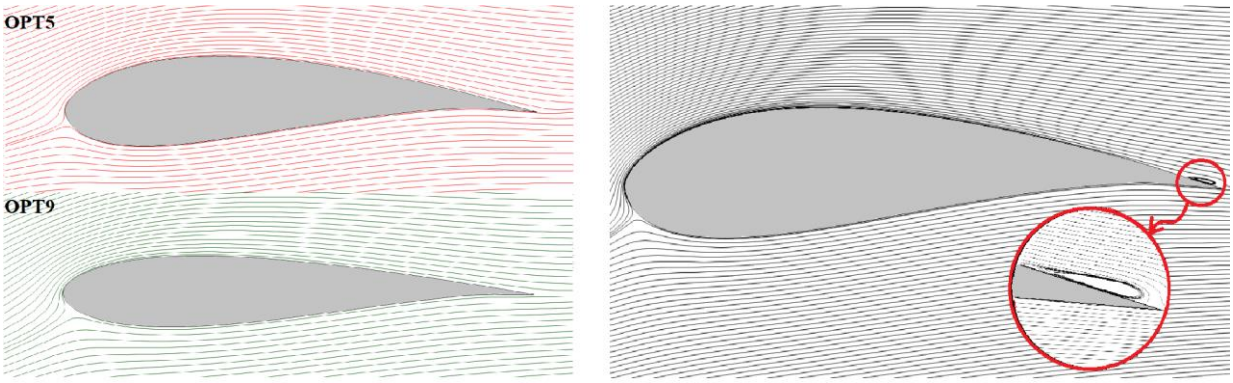

Figure 8. a) Streamlines around the OPT5 and OPT9 airfoils and b) Presence of trailing edge stall on OPT5 for $\boldsymbol{\alpha = 9°}$.

The method's competence in improving efficiency has been evident. However, this analysis is insufficient to understand the real efficiency gain for wind turbine purposes. The appropriate manner to ranking airfoil's performances, neglecting any preference about angles of attack unrelated to aerodynamic efficiency, is tracing their drag polar, then extracting their *E* curves and finally comparing their peak values. Hence, Figure 9 a) represents the drag polar for each optimized airfoil and NACA 0012 from what the *E* curves shown in Figure 9 b) were extracted. As expected, the three different geometries produced different curves, more steeply in the ends. Despite the divergences, all three peaks displayed remarkably similar values, even that they occurred in disparate α.

Because of the acquired camber in contrast to the original symmetric shape, there is an evident vertical offset comparing to NACA 0012 at low angles of attack. Besides, the NACA 0012's maximum *E* occurred at higher α. From all curves, it is noticeable that there was an overall gain in aerodynamic efficiency by the optimization method. It is important to note that single-point optimizations generally have better results when operating at the design flow conditions. Nevertheless, it did not happen in this case, once OPT5 had a higher efficiency for $\alpha = 6.5°$ instead of $\alpha = 5°$. The same fact occurred for OPT7 and OPT9. Even though the differences were minimal, it is a curious phenomenon. It might be explained by the trailing edge adjustment applied over the optimized shapes. Because this modification is not based on gradients, it might have affected the off-design behavior.

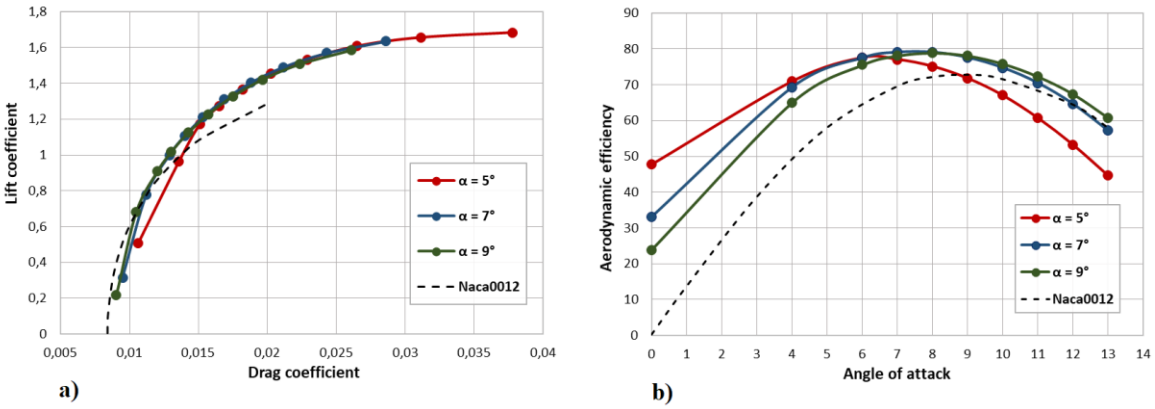

Figure 9. a) Drag polar and b) efficiency curves for optimized and original airfoils.

6. CONCLUSION

In this work computational simulations and the adjoint optimization method was used to optimize the NACA 0012 airfoil to be used as wind turbine blade airfoil. The grid independence study has shown that a C-type mesh with 30 chords of distance for inlet and 50 chords for the outlet produces errors lower than 5% comparing to a twice size mesh, in this case. Besides, it has proved that the first refinement applied was enough for this study. At the validation process, it was possible do verify that the numerical model works properly within the desired regime. The adjoint optimization method was applied for RAE 2822 airfoil and compared with SU2 Test Case results. Despite the mesh differences between the present work and the Test case, a good agreement was observed between the simulations

The optimization method applied in this work succeeded in improving efficiency from an initial airfoil geometry. Trailing edge position adjustments were necessary to maintain reasonable shapes, which has proved to be crucial due to efficiency gain resulted from these modifications. Optimizations were performed, starting from three different angles of attack. The outcomes demonstrated that the optimized geometry is strongly dependent on the initial α. When compared to the initial conditions, the optimization found impressive gains, reaching 7-27% of efficiency improvement. However, regarding the entire airfoils' E curves from a broad range of α, the maximum efficiencies comparisons were less outstanding, namely 6.5 - 8.5%. The best optimization performance was for a starting α of 7º.

For future works, the trailing edge issue should be treated within the code to perform a robust optimization process instead of an afterward adjustment. Moreover, a valuable field for future analyses is a broader investigation of the required features for wind turbine airfoil designs, for example, a smooth stall behavior and roughness independence performance.

7. ACKNOWLEDGEMENTS

Research carried out using the computational resources of the Center for Mathematical Sciences Applied to Industry (CeMEAI) funded by FAPESP (grant 2013/07375-0).

8. REFERENCES

ALLMARAS, S; SPALART, P., A one-equation turbulence model for aerodynamic flows. AIAA Paper, 92-0439, 1992.

CHEN, Jin; WANG, Quan; ZHANG, Shiqiang; EECEN, Peter; GRASSO, Francesco. A new direct design method of wind turbin eairfoils and wind tunnel experiment. ELSEVIER, v. 40, fev. 2016, pp. 2002-2014.

DOUVI, E. C., MARGARIS D.P., “AERODYNAMIC CHARACTERISTICS OF S809 vs. NACA 0012 AIRFOIL FOR WIND TURBINE APPLICATIONS,” 5th International Conference from Scientific Computing to Computational Engineering, Athens, 2012, pp. 1-9.

ECONOMON, Thomas, D. “Constrained shape Design of a Transonic Airfoil at a cte. Cl”, URL: https://su2code.github.io/tutorials/Turbulent_2D_Constrained_RAE2822/ [retrieved 4 Mar. 2020].

GAMBA, Eduardo P.; PALHARINI Rodrigo C. Validação do Modelo Numérico e Determinação das Condições de Escoamento para Simulações CFD na Otimização de Aerofólios de Turbinas Eólicas. Brazil Windpower, oct 2020, pp 1-20.

LADSON, Charles. Effects of Independent Variation of Mach and Reynolds Numbers on the Low-Speed Aerodynamic Characteristics of the NACA 0012 Airfoil Section. NASA Technical Memorandum 4074, Langley Research Center Hampton, Virginia, out. 1988. pp. 25-76.

PALACIOS, Francisco; COLONNO, Michael R.; ARANAKE, Aniket C.; CAMPOS, Alejandro; COPELAND, Sean R.; ECONOMON, Thomas D.; LONKAR, Amrita K.; LUKACZYK, Trent W.; TAYLOR, Thomas W. R.; ALONSO, Juan J. Stanford University Unstructured (SU2): An open-source integrated computational environment for multi-physics simulation and design. Aerospace Sciences Meeting including the New Horizons Forum and Aerospace Exposition, No. AIAA 2013-0287, Dallas, Texas, jan. 2013, pp. 1-60.

POLAT, Ozge; TUNCER, Ismail H. Aerodynamic Shape Optimization of Wind Turbine Blades. ELSEVIER, 2013, p. 28-31.

REUTHER, J. "Aerodynamic Shape Optimization Using Control Theory". RIACS Technical Report 96.09. NASA Ames Research Center. abr. 1996, pp. 1-131.

RIBEIRO, A.F.P.; AWRUCH, A.M.; GOMES, H.M. An airfoil optimization technique for wind turbines. ELSEVIER, v. 36, out. 2012, pp. 4898-4907.

RICHARDSON, L. F. and GAUNT, J. A. The deferred approach to the limit. Part I. Single lattice. Part II. Interpenetrating lattices. Philosophical Transactions of the Royal Society of London. Series A, Containing Papers of a Mathematical or Physical Character, 1997, pp-299-361.

SCHRAMM, M.; STOEVESANDT, B.; PEINKE, J. ADJOINT OPTIMIZATION OF 2D-AIRFOILS IN INCOMPRESSIBLE FLOWS. 1th World Congress on Computational Mechanics, WCCM 2014. Proceedings. Online resource; 5th European Conference on Computational Mechanics (ECCM V); 6th European Conference on Computational Fluid Dynamics (ECFD VI); Barcelona, jul. 2014, pp. 1-12.

SOMERS, Dan M. Design and Experimental Results for the S809 Airfoil. Renewable Energy Laboratory, Golden, Colorado, jan. 1997. pp. 1-97.

SUKRI Mat Al, Mohamed; DOOLAN, Con J.; WHEATLEY, Vincent. GRID CONVERGENCE STUDY FOR A TWO-DIMENSIONAL SIMULATION OF FLOW AROUND A SQUARE CYLINDER AT A LOW REYNOLDS NUMBER. Seventh International Conference on CFD in the Minerals and Process Industries CSIRO, Melbourne, Australia, 11 dez. 2009, pp. 1-6,

WILCOX, D.C., Turbulence Modeling for CFD. 2nd Ed., DCW Industries, Inc., 1998.

9. RESPONSIBILITY NOTICE

The authors are the only responsible for the printed material included in this paper.